Electronic Supplementary Material (ESI) for RSC Advances.
This journal is © The Royal Society of Chemistry 2021

Supplementary Information

The Highly Efficient Removal of HCN over Cu_8Mn_2/CeO_2 Catalytic Material

Zhihao Yi[ab], Jie Sun[*b], Yulin Yang[b], Jigang Li[b], Tian Zhou[b], Shouping Wei[b], Anan Zhu[a]

[a]State Key Laboratory of NBC Protection FOR Civilian, Beijing 102205, China

[b]Department of Chemistry Defense, Institute of NBC Defense, Beijing 102205, China

E-mail: magnsun@mail.tsinghua.edu.cn.

1. Experimental

1.1 Experimental setup

The catalytic materials evaluation device system was shown in Fig. S1. The air purified by four-stage scrubber and HCN with different flow rates were obtained by setting the parameters of the mass flow controller. The water content was adjusted by changing the fraction of air being diverted into the water bubbler placed in a water bath. The HCN flow and air flow was mixed in the mixing chamber, and then the reaction gas consisted of 400 mg/m^3 and 5vol.% H_2O was introduced into the catalytic material bed.

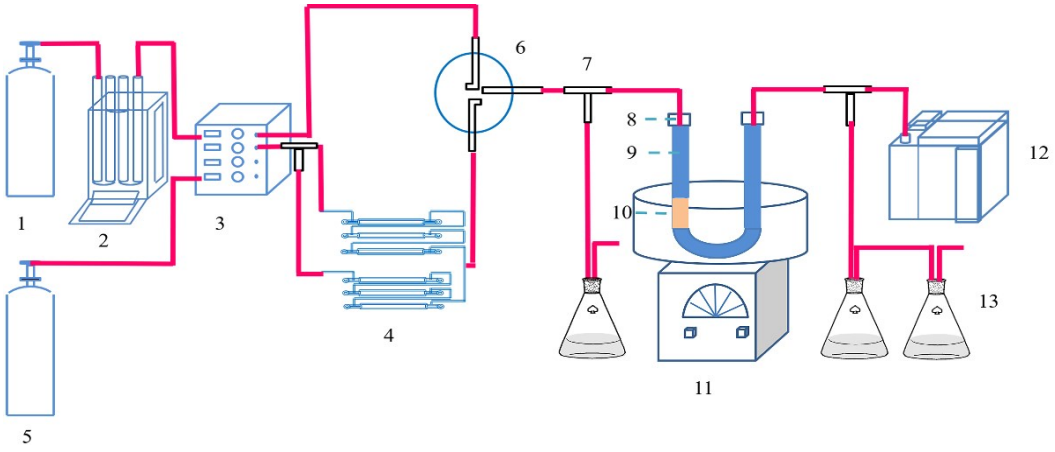

Fig. S1. HCN catalytic reaction flow diagram. 1. Air; 2. Four-stage Scrubber; 3. Mass Flow Controller; 4. Water Vapor Generator; 5. HCN; 6. Mixing Chamber; 7. 3-Way Valve; 8. Asbestos; 9. Quartz Sand; 10. Catalytic Materials; 11. Oil Bath Equipment; 12. Flue Gas Analyzer; 13. Exhaust Absorber.

1.2 Detection and analysis of reacted products

The HCN removal rate and reaction products selectivity were calculated by following equations.

$$X_{HCN} = \left(1 - \frac{C}{C_0}\right) \times 100\% \quad \text{S(1)}$$

$$S_{NH_3} = \frac{C_{NH_3}}{C_0 - C} \times 100\% \quad \text{S(2)}$$

$$S_{NO} = \frac{C_{NO}}{C_0 - C} \times 100\% \quad \text{S(3)}$$

$$S_{NO_2} = \frac{C_{NO_2}}{C_0 - C} \times 100\% \quad \text{S(4)}$$

$$S_{CO} = \frac{C_{CO}}{C_0 - C} \times 100\% \quad \text{S(5)}$$

$$S_{CO_2} = \frac{C_{CO_2}}{C_0 - C} \times 100\% \quad \text{S(6)}$$

$$S_{CN^-} = \frac{C_0 - C - C_{CO_2} - C_{CO}}{C_0 - C} \times 100\% \quad \text{S(7)}$$

$$S_{CO_2} = \frac{1}{2} \frac{C_0 - C - C_{CN^-} - C_{NO} - C_{NO_2} - C_{NH_3}}{C_0 - C} \times 100\% \quad \text{S(8)}$$

where C_0 and C referred to the inlet and outlet concentration of HCN (mg/m^3) respectively.

1.3 Characterization

The morphology and microstructure of prepared samples were examined by the scanning electron microscope (SEM, XL30s-FEG) and transmission electron microscope (TEM, JEM-2001EM).

The XRD patterns of all samples were collected using Rigaku D/max2000 PCX diffractometer using Cu K_α radiation, in the 20~80° 2θ range and with 2°/min scanning speed (λ= 0.15406 nm, operated at 40 kV and 100 mA).

The X-ray photoelectron spectroscopy (XPS) of the samples were performed using EACALAB 250Xi system with monochromatic Al K_α radiation (hv=1486.6 eV) to analyze the surface properties of obtained sample. The sample charging effect was compensated by calibrating the binding energy with adventitious C1s peak at 284.8 eV.

N_2 physisorption measurements were conducted on a Quantachrome Autosorb-iQ instrument, and the specific surface area, pore volumes and average pore diameters were obtained according to the Brunauer-Emmett-Teller (BET) method and Barrett-Joyner-Halenda (BJH) method respectively.

H_2 temperature-programmed reduction (H_2-TPR) experiments were performed using a multifunction chemisorption analyzer (PX200) in a H_2-Ar mixture (10 vol% H_2 ,40 vol% Ar, 40 mL/min). Before the reduction, 50 mg catalyst was pretreated with N_2 at 300 °C for 1 h, and then cooled to ambient temperature. After that the H_2-Ar mixture gas was introduced, and the H_2-TPR profile collected from 100~600 °C at a rate of 10 °C/min.

Fourier-transform infrared spectra (FT-IR) of the samples were recorded on a NEXUS670-FT-IR apparatus over the 4000~400 cm^{-1} wave-number range. Self-supported wafers of 1.3 cm diameter were prepared by pressing 15 mg sample. The wafers were first treated at 250 °C in a flow of high purity He for 0.5 h and then cooled to room temperature.

NH_3 temperature-programmed desorption (NH_3-TPD) was performed on the same Tianjin XQ TP5080 auto-

adsorption apparatus. Prior to the experiments, 150 mg samples were pre-treated at 400 ℃ with He gas for 0.5 h and cooled to room temperature. Then the samples were saturated by 50 mL/min 10 vol.% NH_3 flow at 100 ℃ for 1 h, followed by N_2 purging for 1 h to remove the absorbed ammonium. Finally, the NH_3-TPD was measured from 100 to 800 ℃.

Thermogravimetric analysis (TGA) and differential scanning calorimetry (DSC) were carried out on a DSC 214 Polyma system under flowing air at 100 mL/min and a heating rate of 10 °C/min from 50 to 700 °C.

Inductive coupled plasma optical emission spectros-copy (ICP-OES) were performed on a Pe Avio200 system. Before test, the sample was dissolved in 1 mL HNO_3 and 3 mL HCl solution and then dried at 80 °C. After sieving, the final sample was prepared into 5% acid solution.

2 Results and discussion

2.1 Catalytic activity of CeO_2 loaded with different Cu/Mn ratio

The HCN removal rate over Cu_xMn_y/CeO_2 samples including Cu_8Mn_2/CeO_2, Cu_6Mn_4/CeO_2, Cu_4Mn_6/CeO_2 and Cu_2Mn_8/CeO_2 were displayed in Fig. S2. Besides, the catalytic activity of CuO/CeO_2 and MnO_x/CeO_2 were also studied. As presented in Fig. S2, the catalytic activity of the prepared samples at the whole reaction temperature followed this order: Cu_8Mn_2/CeO_2>Cu_6Mn_4/CeO_2>Cu_4Mn_6/CeO_2>CuO/CeO_2>Cu_2Mn_8/CeO_2>MnO_x/CeO_2. It could be concluded the CuO phase played an important role in the HCN catalytic removal. When MnO_x species were introduced into the CuO/CeO_2, all samples except Cu_2Mn_8/CeO_2 exhibited enhanced catalytic removal ability toward HCN. The lower catalytic activity of Cu_2Mn_8/CeO_2 was attributed to the low CuO loading. According to the experimental results, the optimal Cu/Mn mass ratio was 8/2.

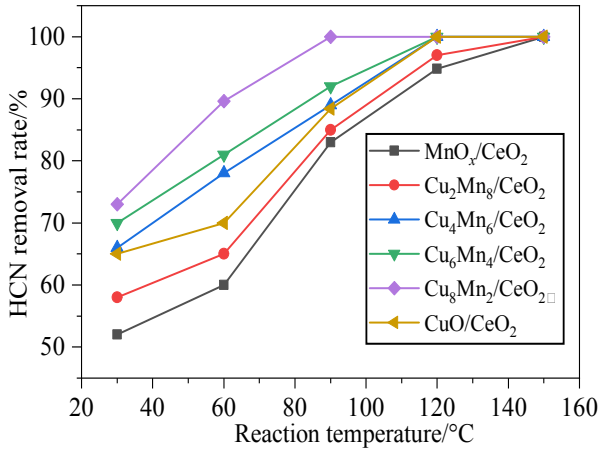

Fig. S2 The HCN removal rate over CeO_2 loaded with different Cu/Mn mass ratio. Reaction condition: 120000h^{-1}, 5 vol.% H_2O.

2.2 Catalytic activity of CeO_2 loaded with different bimetal oxides

Table S1 Comparison of HCN catalytic removal activity over various catalysts

Catalysts	HCN concentration	GHSV/h^{-1}	$T_{100\%}$/°C	References
TiO_2	50 ppm	52 000	350	1
AC–Cu–CoSPc–Ce	100 ppm	32 000	200	2
Cu-Mn-O	160 ppm	25 000	120	3
La_1Cu_9/TiO_2	200 ppm	32 000	150	4

H-ZSM-5	50 ppm	52 000	500	1
Cu-ZSM-5	1200 ppm	20 000	350	5
Cu_8Mn_2/CeO_2	400 mg/m^3	120 000	90	Present work

2.2 Thermal stability of Cu_8Mn_2/CeO_2

To investigate the thermal stability of Cu_8Mn_2/CeO_2 for HCN removal, the Cu_8Mn_2/CeO_2 samples were firstly pretreated at corresponding temperature (200 °C, 400 °C and 600 °C) for 2 h in the muffle furnace, and then tested for the HCN removal in the fixed-bed reactor. As shown in Fig. S3, it could be observed the catalytic activity of Cu_8Mn_2/CeO_2 was not influenced when pretreated temperature varied. The TG-DCS analysis were shown in Fig. S4. It could be observed the Cu_8Mn_2/CeO_2 had negligible weight loss between 50~700 °C in the TGA curve, indicating the samples exhibited excellent thermal stability. The peak at around 500 °C in the DSC curve might be attributed to the oxidation $Cu(NO_3)_2$ to CuO, however, it had no effect on the activity of the Cu_8Mn_2/CeO_2.

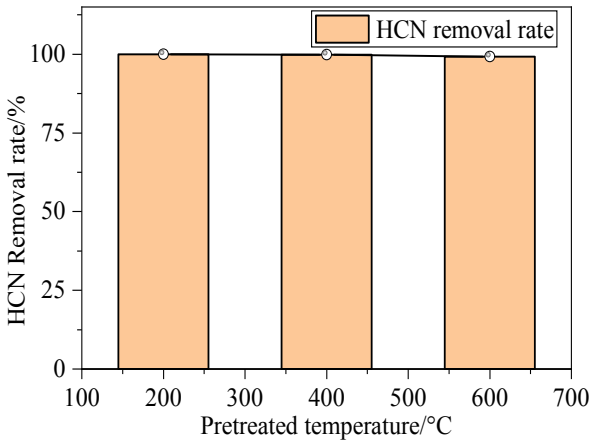

Fig. S3 The HCN removal rate overCu_8Mn_2/CeO_2 pretreated at different temperature. Reaction condition: 120000h^{-1}, 5 vol.% H_2O, 120 °C.

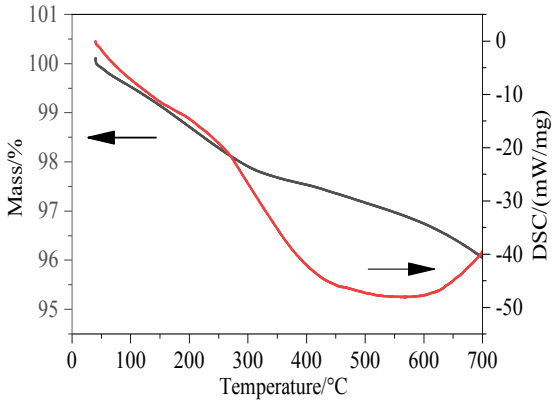

Fig. S4 The TGA-DSC profiles of Cu_8Mn_2/CeO_2.

2.3 Stability of the Cu_8Mn_2/CeO_2 in multiple cycles

To evaluate the behavior of Cu_8Mn_2/CeO_2 under recycling in consecutive catalytic runs, the samples were regenerated after calcinated at 450 °C for 4 h .As shown in Fig. S5, the catalytic activity of Cu_8Mn_2/CeO_2 decreased

slightly as recycling runs increased. The Cu_8Mn_2/CeO_2 could still achieve nearly 90% HCN removal rate even after 4 runs.

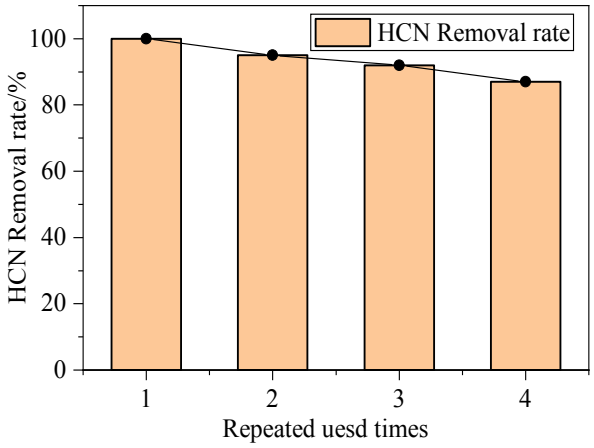

Fig. S5 The HCN removal rate over Cu_8Mn_2/CeO_2 at different repeated used times. Reaction condition: 120000h^{-1}, 5 vol.% H_2O, 120 °C.

2.4 Analysis of HCN reaction products over Cu_8Mn_2/CeO_2

Then reaction products concentration of HCN over Cu_8Mn_2/CeO_2 was listed in Table S1.

Table S2 The balance data of C and N elements

Temperature/°C	The concentration of the reaction products/(mg/m^3)								
	CO	CO_2	NH_3	NO	NO_2	CN^-	N_2	HCN_{inlet}	HCN_{outlet}
30	3	35	3.5	0	0	254	17.3	400	108
60	7.6	209	19.4	4.3	0	143.4	96.5	400	40
90	0	356	34.8	15.2	5.6	44	150.2	400	0
120	0	400	47.2	16.4	19.2	0	158.6	400	0
150	0	400	59.6	0	8.4	0	166	400	0

2.5 Breakthrough behaviors of HCN over Cu_8Mn_2/CeO_2

Fig. S6 showed the breakthrough behaviors of HCN over Cu_8Mn_2/CeO_2 samples at the temperature region of 0~30 °C. It could be observed the breakthrough time (C/C_0 was below 0.1) of HCN over Cu_8Mn_2/CeO_2 decreased as temperature increased. When the temperature was below 10 °C, the breakthrough curve changed not obviously. However, with temperature increased further, the breakthrough curve became steeper and the breakthrough time got shorter. In our previous studies, the breakthrough time of HCN over CuO/CeO_2 increased as temperature increased from 15 °C to 30 °C.[6] The different results between CuO/CeO_2 and Cu_8Mn_2/CeO_2 could be attributed to the following reason: the HCN concentration in our previous studies was 136 mg/m^3, much lower than the HCN (400 mg/m^3) used in this experiment, as temperature increased, the number of activated HCN increased further and accelerated the saturation of activated sites of Cu_8Mn_2/CeO_2, leading the breakthrough time becoming shorter. While the HCN concentration was 136 mg/m^3, the saturation rate of activated sites was much slower, in addition, the catalytic activity of CuO/CeO_2 also promoted the conversion of CN^-, which leading the breakthrough time of HCN increased as temperature increasing.

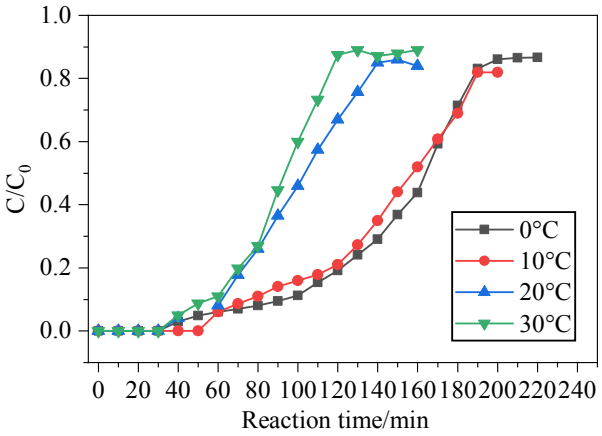

Fig. S6 The HCN removal rate over CeO_2, CuO/CeO_2, MnO_x/CeO_2 and Cu_8Mn_2/CeO_2 samples.

Table S3 The parameters of Yoon and Nelson model for HCN adsorption on Cu_8Mn_2/CeO_2

Temperature/°C	k/min^{-1}	τ/min^{-1}	R^2
10	-0.0354	157	0.999
20	-0.04845	104.3	0.994
30	-0.06194	93.8	0.981

2.6 SEM analysis of the CeO_2 loaded with different bimetal oxides

The SEM images for Cu_8Zn_2/CeO_2, Cu_8Ni_2/CeO_2, Cu_8Co_2/CeO_2, Cu_8Fe_2/CeO_2 and Cu_8Ag_2/CeO_2 were shown in Fig. S7. It could be observed all samples exhibited monodisperse spherical particles and the porous structure of CeO_2 was covered by the metal oxides. The EDS analysis was conducted to investigate the actual loading of metal oxides on CeO_2 support, which was shown in Fig. S8.

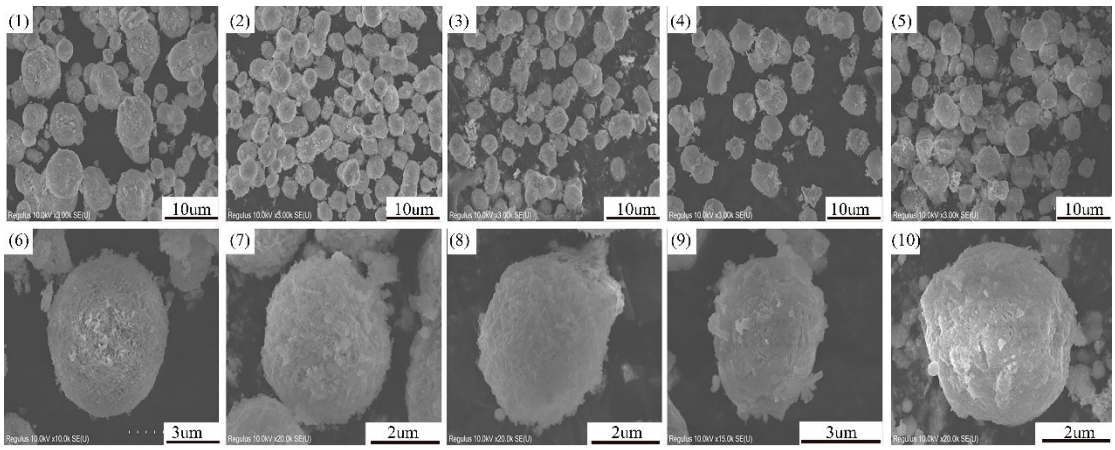

Fig. S7 The SEM images of CeO_2 loaded with different bimetal oxides, (1) (6) Cu_8Zn_2/CeO_2; (2) (7) Cu_8Ni_2/CeO_2; (3) (8) Cu_8Co_2/CeO_2; (4) (9) Cu_8Fe_2/CeO_2; (5) (10) Cu_8Ag_2/CeO_2.

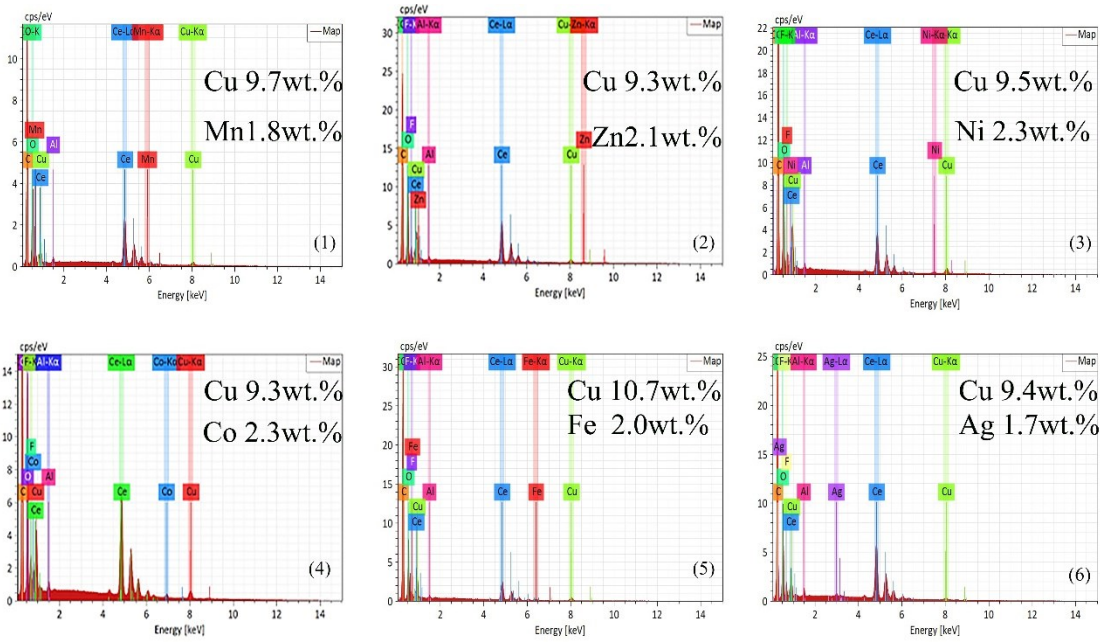

Fig. S8 The EDS analysis of CeO_2 loaded with different bimetal oxides (1) Cu_8Mn_2/CeO_2; (2) Cu_8Zn_2/CeO_2; (3) Cu_8Ni_2/CeO_2; (4) Cu_8Co_2/CeO_2; (5) Cu_8Fe_2/CeO_2; (6) Cu_8Ag_2/CeO_2.

2.7 XRD analysis

The XRD patterns of CeO_2, CuO/CeO_2 and MnO_x/CeO_2 were shown in Fig. S9. For CuO/CeO_2, the two obvious characteristic diffraction peaks of CuO at 35.4 ° and 38.7 ° belonged to the (002), (311) crystal planes.[7] It could be observed a diffraction peak at 37.3 ° in the MnO_x/CeO_2, which was attributed to the Mn_2O_3.[8,9]

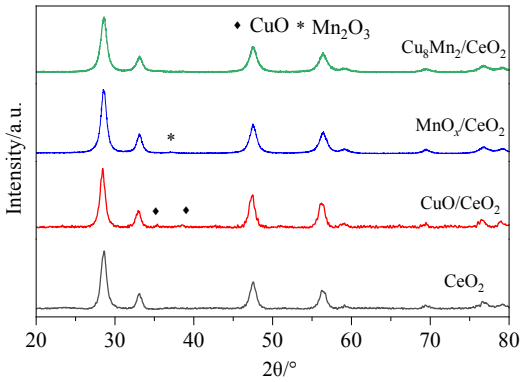

Fig. S9 The XRD patterns of CeO_2, CuO/CeO_2, MnO_x/CeO_2 and Cu_8Mn_2/CeO_2 samples.

2.8 H_2-TPR

Table S4 Temperature of peaks position and quantitative analysis of H_2 consumption

Samples	Peak temperature/°C				H_2 consumption/(cm^3/g)
	Ⅰ	Ⅱ	Ⅲ	Ⅴ	
CuO/CeO_2	158	181	212		27.67
Cu_8Mn_2/CeO_2	164	183	228	274	32.95

2.9 NH_3-TPD

Table S5 The quantitative analysis of desorbed NH_3 at corresponding temperature region.

Samples	Region and NH_3 desorption（100%）		
	100~200 °C	200~500 °C	Above 500 °C
CeO_2	46	14	40
CuO/CeO_2	35	65	—
MnO_x/CeO_2	1	41	58
Cu_8Mn_2/CeO_2	48	16	38

2.10 XRD and ICP analysis

The XRD and ICP analysis were also conducted to further investigate the performance of Cu_8Mn_2/CeO_2 in the reaction system. Fig. S10 displayed the XRD spectra of Cu_8Mn_2/CeO_2 before and after reaction. It could be observed the diffraction peaks corresponding to CeO_2 were not influenced and the CuO and MnO_x's peak still could not be founded, which indicating the CuO and MnO_x always had high dispersion on the CeO_2 support. After reacted with HCN, the content of Cu, Mn changed little according to the XRD results, indicating the Cu_8Mn_2/CeO_2 exhibited high stability in the reaction system.

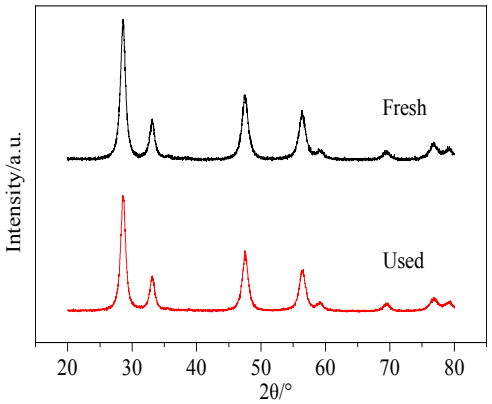

Fig. S10 The XRD patterns of fresh and used Cu_8Mn_2/CeO_2, the used Cu_8Mn_2/CeO_2 referred to samples reacted at 120 °C.

Table S6 The ICP analysis of fresh and used Cu_8Mn_2/CeO_2

Samples	Cu_8Mn_2/CeO_2	
	Cu/wt.%	Mn wt.%
Fresh	7.81	7.69
used[a]	2.1	2.05

[a]Cu_8Mn_2/CeO_2 reacted at 120 °C

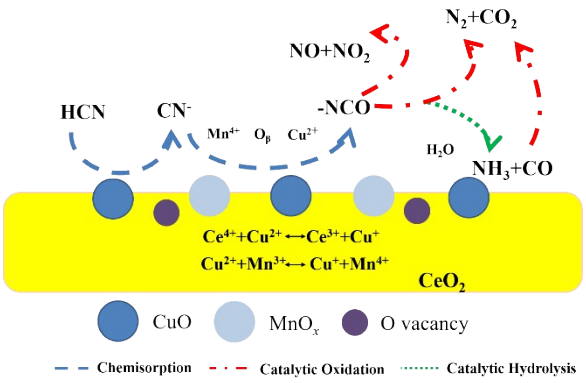

Fig. S11 The schematical diagram of the HCN reaction mechanism over Cu_8Mn_2/CeO_2.

Reference

1 O. KROCHER and M. ELSENER, Hydrolysis and oxidation of gaseous HCN over heterogeneous catalysts, *Appl. Catal. B.,* 2009, 92, 75-89.

2 L.L. Wang, X.Q. Wang and X.L. Jing, Efficient removal of HCN through catalytic hydrolysis and oxidation on Cu/CoSPc/Ce metal-modified activated carbon under low oxygen conditions, *RSC Advances.*, 2016, 6, 113834-113843.

3 Y.J. Li, H. Yang, Y.C. Zhang, J. Hu, J.H. Huang, P. Ning and S.L. Tian, Catalytic decomposition of HCN on copper manganese oxide at low temperatures: Performance and mechanism, *Chem. Eng. J.,* 2018, 346, 621-629.

4 Q. Wang, X. Wang, L. Wang, Y.N. Hu, P. Ning, Y. X. Ma and L. M. Tan, Catalytic oxidation and hydrolysis of HCN over La_xCu_y/TiO_2 catalysts at low temperatures, *Microporous. Mesoporous. Mater.*, 2019, 282, 260-268.

5 N. Liu, X.N. Yuan, B.H. Chen, Y.X. Li and R.D. Zhang, Selective catalytic combustion of hydrogen cyanide over metal modified zeolite catalysts: From experiment to theory, *Catal. Today.*, 2017, 297, 201-210.

6 Z.H. Yi, J. Sun, J.G. Li, T. Zhou, S P. Wei, H.J. Xie and Y.L. Yang, High efficient removal of HCN over porous CuO/CeO_2 micro-nano spheres at lower temperature range, *Chin. J. Chem. Eng.*, 2020, Doi: 10.1016/j.cjche.2020.08.029.

7 D. Gamarra, G. Munuera, A.B. Hungría, M.J. Fernández-García, C. Conesa and P.A. Midgley, Structure-activity relationship in nano-structured copper-ceria based preferential CO oxidation catalysts, *J. Phys. Chem. C.*, 2007, 111, 11026-11038.

8 Z. Wang, G.L. Shen, J.Q. Li, H.D. Liu, Q. Wang and Y.F. Chen, Catalytic removal of benzene over CeO_2-MnO_x composite oxides prepared by hydrothermal method, *Appl. Catal. B.*, 2013, 138, 253-259.

9 X.F. Tang, Y.G. Li, X.M. Huang, Y.D. Xu, H.Q. Zhu, J.G. Wang and W.J. Shen, MnO_x-CeO_2 mixed oxide catalysts for complete oxidation of formaldehyde: Effect of preparation method and calcination temperature, *Appl. Catal. B.*, 2006, 62, 265-273.